

Contrastive Learning on Multimodal Analysis of Electronic Health Records

Tianxi Cai^{1,2*}, Feiqing Huang^{1*}, Ryumei Nakada^{3*},
Linjun Zhang^{3*}, Doudou Zhou^{4*}

¹Department of Biostatistics, Harvard T.H. Chan School of Public Health, Boston, MA

²Department of Biomedical Informatics, Harvard Medical School, Boston, MA

³Department of Statistics, Rutgers University, Piscataway, NJ

⁴Department of Statistics and Data Science, National University of Singapore, Singapore

*alphabetical order

Abstract

Electronic health record (EHR) systems capture a wealth of multimodal clinical data, encompassing both structured clinical codes and unstructured clinical notes. Yet, many EHR-focused studies have traditionally examined these modalities in isolation or combined them using simplistic methods. Such approaches reinforce the view of structured and unstructured data as separate, overlooking the intrinsic synergy between them. In reality, these modalities are deeply interconnected, each containing clinically relevant and complementary information that, when integrated effectively, can provide a more comprehensive understanding of patient health. Integrating these modalities enables a richer, more complete representation of a patient’s medical history, offering deeper insights into their health. Despite the great success of multimodal contrastive learning on vision-language, its potential remains under-explored in the realm of multimodal EHR, particularly in terms of its theoretical understanding. To support statistical analysis of multimodal EHR data, we propose a novel multimodal feature embedding generative model and design a multimodal contrastive loss to obtain the multimodal EHR feature representation. Our theoretical analysis demonstrates the effectiveness of multimodal learning compared to single-modality learning and connects the solution of the loss function to the singular value decomposition of a pointwise mutual information matrix. This connection paves the way for a privacy-preserving algorithm tailored for multimodal EHR feature representation learning. Simulation studies show that the proposed algorithm performs well under a variety of configurations. We further validate the clinical utility of the proposed algorithm in real-world EHR data.

Keywords: Natural language processing, textual data, structured data, representation learning, singular value decomposition.

1 Introduction

The growing accessibility of Electronic Health Record (EHR) data presents numerous opportunities for clinical research, ranging from patient profiling (Halpern et al., 2016) to predicting medical events (Choi et al., 2017). However, the complexity increases with the multimodal nature of EHR data, which encompasses diverse data from patient demographics and genetic information to unstructured textual data like clinical notes, as well as structured data such as diagnostic and procedure codes, medication orders, and lab results.

A key challenge in EHR-focused research lies in effectively merging these different data types and ensuring that their clinical aspects are meaningfully and coherently represented. Research has shown the benefits of integrating structured and unstructured data for tasks like automated clinical code assignment (Scheurwegs et al., 2016), managing chronic diseases (Sheikhalishahi et al., 2019), and pharmacovigilance (Stang et al., 2010). While these different modalities serve as complementary data sources, there is significant overlap and correlation among these modalities (Qiao et al., 2019). Joint representation of both structured and narrative data into a more manageable low-dimensional space where similar features are grouped closely can significantly improve the utility of both data types. This representation learning technique has gained popularity for its ability to capture and represent the intricate relationships among various EHR features.

Despite extensive research on EHR feature representation, most studies have focused on datasets with a single modality, including structured (Choi et al., 2016a; Kartchner et al., 2017; Hong et al., 2021; Zhou et al., 2022) and unstructured data (De Vine et al., 2014; Choi et al., 2016b; Beam et al., 2019; Alsentzer et al., 2019; Huang et al., 2020; Lehman and Johnson, 2023). For example, Alsentzer et al. (2019) adapted BERT (Devlin et al., 2019) to the clinical domain by pretraining on MIMIC-III notes (Johnson et al., 2016), a

process that was highly resource-intensive. De Vine et al. (2014) aligned free-text with the UMLS Concept Unique Identifier (CUI) space (McInnes et al., 2007) and applied skip-gram (Mikolov et al., 2013) to learn embeddings, while Choi et al. (2016b), Beam et al. (2019); Hong et al. (2021); Levy and Goldberg (2014); Arora et al. (2016) used singular value decomposition (SVD) on pointwise mutual information (PMI) matrices.

Building on these unimodal advances, recent work has explored multimodal EHR representations that integrate both structured and unstructured information (Khadanga et al., 2019; Zhang et al., 2020; Bardak and Tan, 2021; Gan et al., 2025). Joint representation is preferable to treating all data as a single modality because, although structured codes and unstructured text encode overlapping clinical concepts, they possess fundamentally different statistical forms. Ignoring these cross-modality differences can obscure modality-specific information, discard complementary signal, and amplify systematic bias (see further discussion in Section 3.2). By contrast, multimodal integration can exploit the complementary strengths of distinct modalities, yielding representations that are not only richer but also less biased than those obtained from unimodal analyses. For instance, information that is noisy or missing in one modality may be corroborated by the other, thereby stabilizing estimation and enhancing generalization. In this paper, we develop a theoretical framework (Section 3) and provide empirical evidence (Sections 4 and 5) to demonstrate that multimodal analysis addresses these challenges and produces more reliable and interpretable representations of EHR data.

To address these limitations, Liu et al. (2022) proposed a multimodal pre-trained language model that incorporates a cross-attention mechanism to enrich EHR representations across structured and unstructured domains. More recently, multimodal contrastive learning strategies have also been explored (Li and Gao, 2022; Yin et al., 2023; Wang et al.,

2023). Inspired by the success of vision–language models such as CLIP (Radford et al., 2021), these approaches aim to learn unified representations of heterogeneous data modalities. From a statistical perspective, contrastive learning can be interpreted through the lens of noise-contrastive estimation (Gutmann and Hyvärinen, 2010), in which a parametric score function distinguishes positive’ pairs drawn from the joint distribution from negative’ pairs drawn from the product of marginals. The popular InfoNCE loss (Oord et al., 2018) maximizes a lower bound on mutual information and is closely related to low-rank approximations of the PMI matrix (Levy and Goldberg, 2014). Despite their promise, these methods remain limited by their reliance on deep neural networks, which are often criticized for their “black-box” nature. Practical challenges include the absence of rigorous theoretical guarantees, high computational cost, and privacy concerns due to the need for patient-level data. Together, these issues constrain the applicability of existing multimodal contrastive learning frameworks in the context of EHR data.

While some theoretical analyses of multimodal learning exist, their applicability to sparse discrete EHR data has been limited. Groundbreaking studies like Huang et al. (2021) have illustrated the benefits of multimodal learning, showing that learning across multiple modalities can reduce population risk compared to single-modality methods. Recently, Deng et al. (2023) theoretically proved the zero-shot transfer ability of CLIP. Furthermore, Nakada et al. (2023) explored multimodal contrastive learning’s performance under a spiked covariance model. However, these studies do not directly apply to the unique discrete feature structure of EHR data, leaving an unaddressed theoretical gap in understanding multimodal contrastive learning’s application in healthcare. Bridging this gap is vital, as it lays a foundation for multimodal contrastive learning’s development and implementation in healthcare, maximizing its potential to improve care and drive medical research forward.

Complementary lines of research have attempted to address related challenges from different angles. For instance, exponential family principal component analysis (PCA) (Collins et al., 2001) and nonlinear PCA (Hinton and Salakhutdinov, 2006) extend classical PCA to non-Gaussian and nonlinear settings, while kernel PCA (KPCA) (Gupta et al., 2019) provides additional flexibility. Yet, handling multimodal, sparse, and privacy-sensitive data remains an open challenge. In parallel, the statistical literature on integrative dimension reduction, such as JIVE (Lock et al., 2013), AJIVE (Feng et al., 2018), and other multi-view factor models (Zhou et al., 2015; Yang and Michailidis, 2016; Yi et al., 2023, e.g.), provides tools for modeling shared and modality-specific structures. Our framework shares this goal but is tailored to discrete EHR features and prioritizes privacy-preserving learning via co-occurrence data.

To overcome these limitations, we introduce the **C**ontrastive **L**earning **A**lgorithm for **I**ntegrated **M**ultimodal **E**lectronic health records (CLAIME). Our findings confirm that CLAIME is not only effective for deriving multimodal EHR feature representations but also respects privacy by requiring only aggregated data. Additionally, we propose a novel multimodal feature embedding generative model (2.1) in Section 2.1, designed to enhance statistical analysis of multimodal EHR data. This model is notable for its interpretability and accurate portrayal of EHR data generation. It distinguishes itself from earlier word vector generative models (Arora et al., 2016, 2018; Lu et al., 2023; Xu et al., 2023) by (1) enabling the integration of multimodal EHR features, and (2) allowing patient heterogeneity by incorporating error terms specific to patients, thus increasing the model’s robustness. Within this generative framework, we validate the consistency of the CLAIME algorithm and clarify the relationship between multimodal feature embeddings and a multimodal PMI matrix. The proposed algorithm is also privacy-preserving since it only requires summary-

level data, opening doors for collaboration across multiple institutions. Our research also fills a theoretical void in the analysis of multimodal contrastive learning for EHR data.

The rest of the paper is organized as follows. Section 2 introduces the proposed method, and Section 3 presents its theoretical properties. Sections 4 and 5 provide simulation and real-world evaluations, respectively. Section 6 concludes with a discussion.

2 Method

We begin by defining the notation. For any matrix \mathbf{A} , let $\|\mathbf{A}\|$, $\|\mathbf{A}\|_{\max}$, and $\|\mathbf{A}\|_F$ denote its operator norm, entrywise maximum norm, and Frobenius norm, respectively. Let $\mathbf{P}_p(\mathbf{A})$ be the top- p right singular vectors of \mathbf{A} , chosen arbitrarily if non-unique, and let $s_j(\mathbf{A})$ be its j -th largest singular value. Define $\mathcal{O}_{d,p}$ ($d \geq p$) as the set of $d \times p$ orthonormal matrices. For sequences $\{a_n\}, \{b_n\} > 0$, write $a_n \lesssim b_n$, $a_n = O(b_n)$, $b_n \gtrsim a_n$, or $b_n = \Omega(a_n)$ if $a_n \leq Cb_n$ for some $C > 0$ and all n ; write $a_n \ll b_n$ or $a_n = o(b_n)$ if $a_n/b_n \rightarrow 0$. Let $[I] = \{1, 2, \dots, I\}$ for any positive integer I , and write $a \vee b$ and $a \wedge b$ for $\max(a, b)$ and $\min(a, b)$, respectively. Denote by \mathbf{e}_j the j -th unit vector in \mathbb{R}^d .

2.1 Model Assumptions

Our approach is motivated by real-world EHRs, where structured codes (e.g., diagnoses, medications) and unstructured concepts extracted from clinical notes (e.g., CUIs) offer complementary views of a patient’s health (Figure 1). During a hospital visit, patient i generates two types of data: structured codes and CUIs, which are typically collected by different subsystems and subject to distinct noise processes. For example, structured codes often reflect billing practices, while CUIs are derived from free-text notes via Named Entity Recognition (NER) tools. This data processing pipeline aligns with standard practice for

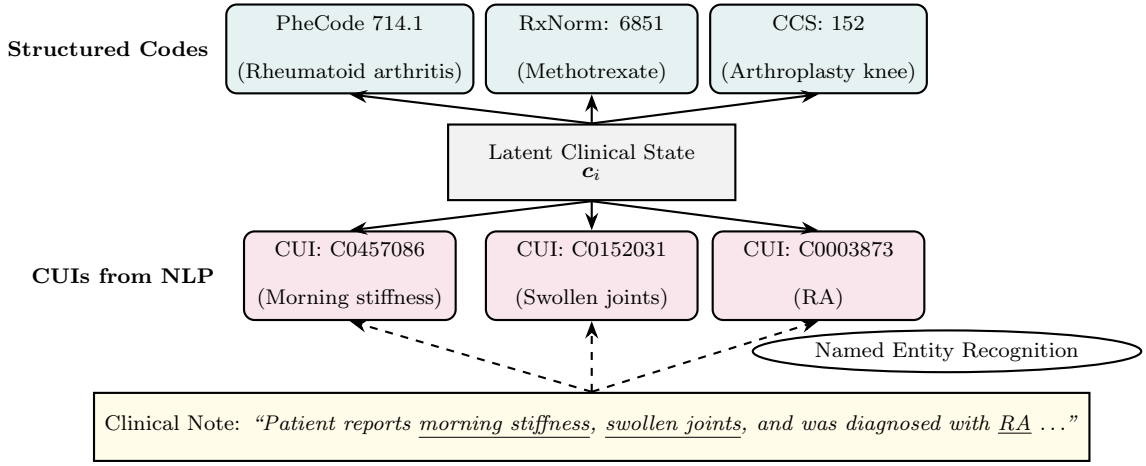


Figure 1: Illustration of multimodal EHR generation: A shared latent state \mathbf{c}_i generates both structured codes (top) and unstructured CUIs (bottom), motivating (2.1).

mapping text to UMLS concepts (Choi et al., 2016b; Beam et al., 2019). We primarily focus on the two-modality case but also discuss extensions to more general multi-modality settings involving three or more modalities below.

Accordingly, for each patient i , we observe two sets of features: $\{w_{i,t}^{(1)}\}_{t=1}^{T_i^{(1)}}$ for structured codes and $\{w_{i,t}^{(2)}\}_{t=1}^{T_i^{(2)}}$ for CUIs, where $w_{i,t}^{(1)} \in \mathcal{W}^{(1)}$ and $w_{i,t}^{(2)} \in \mathcal{W}^{(2)}$. Let $\mathcal{W}^{(1)} := [d_1]$ and $\mathcal{W}^{(2)} := [d] \setminus [d_1]$, where $d = d_1 + d_2$ denotes the total number of distinct features across both modalities. To model the generative process of these features, we adopt the following latent variable model, which captures the shared structure between modalities while allowing for modality-specific noise:

$$\begin{aligned} \mathbb{P}(w_{i,t}^{(1)} = w \mid \mathbf{c}_i, \boldsymbol{\epsilon}_i^{(1)}) &= \frac{\exp(\langle \mathbf{v}_w^*, \mathbf{c}_i \rangle + \epsilon_{i,w}^{(1)})}{\sum_{w' \in \mathcal{W}^{(1)}} \exp(\langle \mathbf{v}_{w'}^*, \mathbf{c}_i \rangle + \epsilon_{i,w'}^{(1)})}, \quad w \in \mathcal{W}^{(1)}, t \in [T_i^{(1)}], \\ \mathbb{P}(w_{i,t}^{(2)} = w \mid \mathbf{c}_i, \boldsymbol{\epsilon}_i^{(2)}) &= \frac{\exp(\langle \mathbf{v}_w^*, \mathbf{c}_i \rangle + \epsilon_{i,w}^{(2)})}{\sum_{w' \in \mathcal{W}^{(2)}} \exp(\langle \mathbf{v}_{w'}^*, \mathbf{c}_i \rangle + \epsilon_{i,w'}^{(2)})}, \quad w \in \mathcal{W}^{(2)}, t \in [T_i^{(2)}]. \end{aligned} \quad (2.1)$$

Here, $\mathbf{c}_i \sim \mathcal{N}(\mathbf{0}, \mathbf{I}_p)$ represents the latent clinical state of patient i , and $\mathbf{v}_w^* \in \mathbb{R}^p$ is the ground-truth embedding of feature w . The modality-specific noise vectors $\boldsymbol{\epsilon}_i^{(M)} = (\epsilon_{i,w}^{(M)})_{w \in \mathcal{W}^{(M)}} \sim \mathcal{N}(\mathbf{0}, \boldsymbol{\Sigma}_M)$, for $M \in \{1, 2\}$, capture variability not explained by the latent

state, such as documentation inconsistencies or NLP extraction errors.

This formulation reflects our core assumption: while structured and unstructured features are conditionally generated from a shared latent representation \mathbf{c}_i , they are distorted independently by modality-specific noise. The model thus supports: (1) integration of heterogeneous EHR data sources, (2) robustness to differing noise structures across modalities, and (3) inference of informative embeddings from only summary-level statistics.

Remark 2.1. The assumption $\mathbf{c}_i \sim N(\mathbf{0}, \mathbf{I}_p)$ is used to support theoretical analysis, not as a requirement for the CLAIME algorithm itself. Our method does not rely on estimating individual \mathbf{c}_i vectors. Instead, the Gaussian assumption enables analytical tractability in characterizing the expected co-occurrence patterns of EHR features, which in turn justify the use of SVD-based estimators in later sections. Similar analytical approximations have been derived under alternative latent structures, such as unit sphere random walks (Arora et al., 2016, 2017) or scaled-Gaussian priors (Xu et al., 2023). Finally, due to the rotational invariance of our model, the identity covariance assumption on \mathbf{c}_i can be relaxed without affecting the core methodology.

2.2 The CLAIME Algorithm

We define code and CUI embedding matrices as $\mathbf{V}_1^* = (\mathbf{v}_1^*, \dots, \mathbf{v}_{d_1}^*)^\top \in \mathbb{R}^{d_1 \times p}$ and $\mathbf{V}_2^* = (\mathbf{v}_{d_1+1}^*, \dots, \mathbf{v}_{d_1+d_2}^*)^\top \in \mathbb{R}^{d_2 \times p}$, respectively, and aim to infer $\mathbf{V}^* = (\mathbf{V}_1^{*\top}, \mathbf{V}_2^{*\top})^\top \in \mathbb{R}^{d \times p}$. The embeddings are intended to reflect clinical semantics, meaning that highly similar (e.g., rheumatoid arthritis and juvenile rheumatoid arthritis) or related (e.g., fasting glucose and type II diabetes) EHR entities should be embedded close to each other.

To motivate our algorithm design, recall that model (2.1) assumes EHR features from both modalities are generated from a shared latent patient embedding \mathbf{c}_i . This implies that

features frequently co-occurring within the same patient are likely conditionally dependent through \mathbf{c}_i , and should have similar embeddings, whereas features from different patients are marginally independent and their embeddings should remain unaligned.

Before introducing our algorithm, we first define aggregate co-occurrence matrices $\mathbf{C}^{(M,M)}$ and $\mathbf{D}^{(M,M')}$ for $M, M' \in \{1, 2\}$ across different modalities as:

$$\mathbf{C}^{(M,M)}(w, w') = \sum_{i=1}^n \mathbf{C}_{i,i}^{(M,M)}(w, w'), \quad \mathbf{D}^{(M,M')}(w, w') = \sum_{i=1}^n \mathbf{D}_{i,i}^{(M,M')}(w, w')$$

where $\mathbf{C}_{i,j}^{(M,M)}(w, w') = |\{(t, s) \in [T_i^{(M)}] \times [T_j^{(M)}] : t \neq s, w_{i,t}^{(M)} = w, w_{j,s}^{(M)} = w'\}|$ and $\mathbf{D}_{i,j}^{(M,M')}(w, w') = |\{(t, s) \in [T_i^{(M)}] \times [T_j^{(M')}] : w_{i,t}^{(M)} = w, w_{j,s}^{(M')} = w'\}|$ for $i, j \in [n]$. Further, we define the marginal occurrence count of $w \in \mathcal{W}^{(M)}$ as:

$$\gamma_w^{(M)} = \mathbf{C}^{(M,M)}(w, \cdot) = \sum_{w' \in \mathcal{W}^{(M)}} \mathbf{C}^{(M,M)}(w, w'). \quad (2.2)$$

To derive clinically meaningful embeddings that reflect modality-specific co-occurrence patterns, we propose a contrastive learning algorithm aligned with model (2.1). Contrastive learning encourages embeddings of positive pairs to be similar and those of negative pairs to be dissimilar. In our setting, code-CUI pairs from the same patient are treated as positive, while pairs from different patients as negative. This naturally aligns with our generative assumptions and enables learning from aggregated co-occurrence data. Specifically, we define the multimodal contrastive learning loss as

$$\mathcal{L}_{\text{CLAIME}}(\mathbf{V}_1, \mathbf{V}_2) = \frac{\sum_{i,j:i \neq j} s_{ij}}{n(nS_1^{(1)}S_1^{(2)} - S_2^{(1,2)2})} - \frac{\sum_{i=1}^n s_{ii}}{nS_2^{(1,2)2}} + \frac{\lambda}{2} \|\mathbf{V}_1 \mathbf{V}_2^\top\|_F^2, \quad (2.3)$$

where $s_{ij} = \sum_{t \in [T_i^{(1)}]} \sum_{s \in [T_j^{(2)}]} \frac{\langle \mathbf{v}_{w_{i,t}^{(1)}}, \mathbf{v}_{w_{j,s}^{(2)}} \rangle}{\gamma_{w_{i,t}^{(1)}}^{(1)} \gamma_{w_{j,s}^{(2)}}^{(2)}}$. Here, $\mathbf{V}_1 = (\mathbf{v}_1, \dots, \mathbf{v}_{d_1})^\top \in \mathbb{R}^{d_1 \times p}$ and $\mathbf{V}_2 = (\mathbf{v}_{d_1+1}, \dots, \mathbf{v}_{d_1+d_2})^\top \in \mathbb{R}^{d_2 \times p}$, $\lambda > 0$ serves as a regularization coefficient, $\gamma_w^{(M)}$, $M = 1, 2$ are weights chosen based on the frequency of w , as defined in (2.2). The quantities $S_q^{(M)} = (n^{-1} \sum_{i=1}^n (T_i^{(M)})^q)^{1/q}$ and $S_q^{(1,2)} = (n^{-1} \sum_{i \in [n]} (T_i^{(1)})^{q/2} (T_i^{(2)})^{q/2})^{1/q}$ for $q \geq 1$ are

empirical moments and cross-moments of $T_i^{(M)}$, and correspond to the number of terms in the two summation components of the loss. Our analysis in Section 3 motivates the choice of $\gamma_w^{(M)}$ to guide the minimizer towards \mathbf{V}^* .

This loss encourages code-CUI pairs that co-occur within the same patient (second term) to be closely embedded, while penalizing similarity between pairs from different patients (the first term). The regularization term $\frac{\lambda}{2}\|\mathbf{V}_1\mathbf{V}_2^\top\|_F^2$ ensures numerical stability and controls the embedding magnitude. By optimizing this loss, the model learns to align embeddings based on co-occurrence patterns, which signal shared clinical relevance.

To efficiently obtain $\widehat{\mathbf{V}} = (\widehat{\mathbf{V}}_1^\top, \widehat{\mathbf{V}}_2^\top)^\top = \arg \min \mathcal{L}_{\text{CLAIME}}(\mathbf{V}_1, \mathbf{V}_2)$, we define normalized count vectors for each patient i and modality $M \in \{1, 2\}$: $\mathbf{w}_i^{(M)} \in \mathbb{R}^{d_M}$ with $\mathbf{w}_{i,w}^{(M)} = \frac{1}{\gamma_w^{(M)}} \sum_{t \in [T_i^{(M)}]} \mathbb{I}(w_{i,t}^{(M)} = w)$. The patient-level representation for each modality becomes $\mathbf{V}_1^\top \mathbf{w}_i^{(1)}$ and $\mathbf{V}_2^\top \mathbf{w}_i^{(2)} \in \mathbb{R}^p$. Using this, the loss (2.3) (excluding regularization) can be expressed by pair-wise co-occurrences of concepts as:

$$\begin{aligned} & \frac{1}{n(nS_1^{(1)}S_1^{(2)} - S_2^{(1,2)2})} \sum_{w=1}^{d_1} \sum_{w'=d_1+1}^{d_1+d_2} \frac{\langle \mathbf{v}_w, \mathbf{v}_{w'} \rangle}{\gamma_w^{(1)} \gamma_{w'}^{(2)}} \sum_{i=1}^n \sum_{j:j \neq i}^n \sum_{t \in [T_i^{(1)}]} \sum_{s \in [T_j^{(2)}]} \mathbb{I}(w_{i,t}^{(1)} = w) \mathbb{I}(w_{j,s}^{(2)} = w') \\ & - \frac{1}{nS_2^{(1,2)2}} \sum_{w=1}^{d_1} \sum_{w'=d_1+1}^{d_1+d_2} \frac{\langle \mathbf{v}_w, \mathbf{v}_{w'} \rangle}{\gamma_w^{(1)} \gamma_{w'}^{(2)}} \sum_{i=1}^n \sum_{t \in [T_i^{(1)}]} \sum_{s \in [T_i^{(2)}]} \mathbb{I}(w_{i,t}^{(1)} = w) \mathbb{I}(w_{i,s}^{(2)} = w') \\ & = \frac{1}{n(nS_1^{(1)}S_1^{(2)} - S_2^{(1,2)2})} \sum_{i=1}^n \sum_{j:j \neq i}^n (\mathbf{V}_1^\top \mathbf{w}_i^{(1)})^\top (\mathbf{V}_2^\top \mathbf{w}_j^{(2)}) - \frac{1}{nS_2^{(1,2)2}} \sum_{i=1}^n (\mathbf{V}_1^\top \mathbf{w}_i^{(1)})^\top (\mathbf{V}_2^\top \mathbf{w}_i^{(2)}). \end{aligned}$$

The first term captures the average similarity of negative (cross-patient) pairs, while the second reflects positive (same-patient) pairs. Minimizing this loss encourages within-patient alignment while discouraging cross-patient alignment. Subsequently, via arguments given in Supplementary S2, we have the following proposition.

Proposition 2.1. *We have*

$$\mathcal{L}_{\text{CLAIME}}(\mathbf{V}_1, \mathbf{V}_2) = \frac{\lambda}{2} \left\| \mathbf{V}_1 \mathbf{V}_2^\top - \frac{1}{\lambda} \widehat{\text{PMI}}_{\text{CLAIME}} \right\|_F^2 + (\text{constant}),$$

where $\widehat{\text{PMI}}_{\text{CLAIME}} = \{\widehat{\text{PMI}}_{\text{CLAIME}}(w, w')\}_{w \in \mathcal{W}^{(1)}, w' \in \mathcal{W}^{(2)}}$ with

$$\widehat{\text{PMI}}_{\text{CLAIME}}(w, w') := \frac{\mathbf{C}^{(1,1)}(\cdot, \cdot) \mathbf{C}^{(2,2)}(\cdot, \cdot)}{\mathbf{C}^{(1,1)}(w, \cdot) \mathbf{C}^{(2,2)}(w', \cdot)} \left(\frac{\mathbf{D}^{(1,2)}(w, w')}{\mathbf{D}^{(1,2)}(\cdot, \cdot)} - \frac{\mathbf{C}^{(c)}(w, w')}{n(nS_1^{(1)}S_1^{(2)} - S_2^{(1,2)2})} \right),$$

and $\mathbf{C}^{(c)}(w, w') = \sum_{i=1}^n \sum_{j:j \neq i}^n \mathbf{D}_{i,j}^{(1,2)}(w, w')$.

Proposition 2.1 shows that $\mathcal{L}_{\text{CLAIME}}(\mathbf{V}_1, \mathbf{V}_2)$ reduces to a rank-constrained approximation of an empirical association matrix $\widehat{\text{PMI}}_{\text{CLAIME}}$, where each entry $\widehat{\text{PMI}}_{\text{CLAIME}}(w, w')$ quantifies the association between features w and w' . Section 3 establishes that this matrix converges to the population-level PMI matrix under mild assumptions.

To estimate the embeddings, we compute the rank- p SVD of $\widehat{\text{PMI}}_{\text{CLAIME}}$, denoted as $\widehat{\mathbf{U}}_1 \widehat{\mathbf{\Lambda}} \widehat{\mathbf{U}}_2^\top$, where $\widehat{\mathbf{U}}_1 \in \mathbb{R}^{d_1 \times p}$ and $\widehat{\mathbf{U}}_2 \in \mathbb{R}^{d_2 \times p}$ are the matrices of left and right singular vectors, respectively, and $\widehat{\mathbf{\Lambda}} \in \mathbb{R}^{p \times p}$ is a diagonal matrix with its diagonal elements being the top p singular values. Then, we set $\widehat{\mathbf{V}}_1 = \widehat{\mathbf{U}}_1 \widehat{\mathbf{\Lambda}}^{1/2}$ and $\widehat{\mathbf{V}}_2 = \widehat{\mathbf{U}}_2 \widehat{\mathbf{\Lambda}}^{1/2}$. From Proposition 2.1, the scalar λ in (2.3) controls the scale of the embeddings via the magnitude of singular values, but not their subspace. Since downstream similarity metrics like cosine similarity are scale-invariant, we may fix $\lambda = 1$ for simplicity.

Our formulation is inspired by contrastive learning, which promotes high similarity among positive pairs and low similarity among negatives. Unlike vision-language models such as CLIP (Radford et al., 2021), it operates on discrete, high-dimensional EHR features rather than continuous image or text embeddings, and relies only on aggregated co-occurrence statistics instead of raw patient-level data.

Remark 2.2 (Nonlinear extension). The CLAIME framework can be naturally extended to a softmax-based contrastive loss similar to that used in CLIP:

$$\mathcal{L}'_{\text{CLAIME}}(\mathbf{V}_1, \mathbf{V}_2) = -\frac{1}{n(S_2^{(1,2)})^2} \sum_{i=1}^n T_i^{(1)} T_i^{(2)} \log \frac{\exp(s_{ii}/(T_i^{(1)} T_i^{(2)} \eta))}{\sum_{j:j \neq i} T_i^{(1)} T_j^{(2)} \exp(\alpha_i s_{ij}/(T_i^{(1)} T_j^{(2)} \eta))} + R'(\mathbf{V}_1, \mathbf{V}_2), \quad (2.4)$$

where R' is a smooth regularizer, $\eta > 0$ the temperature, and α_i depends on $(T_i^{(M)})_{i \in [n], M=1,2}$. In the high-temperature limit ($\eta \rightarrow \infty$), the loss reduces to the linear CLAIME loss (2.3), up to a constant and regularization. Details are provided in Supplementary S2.2.

Remark 2.3 (Extending CLAIME to more than two modalities). EHR data often consist of multiple heterogeneous streams. For instance, codified data alone encompass diagnoses, procedures, medications, and laboratory results, each of which can be treated as a distinct modality. Similarly, NLP-derived CUIs can be partitioned by semantic types such as *Disease or Syndrome* and *Diagnostic Procedure*. To accommodate such settings, we generalize CLAIME beyond two modalities in Supplementary S6 by estimating cross-modal PMI matrices for every pair of modalities and jointly learning embeddings over all sources. Further extensions to continuous-valued sources such as genomics, imaging, or clinical tests will require suitable generative models for continuous data.

2.3 Comparison between CLAIME and Baseline Approaches

We next contrast CLAIME with the baseline approaches of ignoring between-modality differences. Dealing with multimodal data often presents difficulties, leading to conventional methods that overlook the differences between various modalities. A basic strategy commonly adopted is to simply merge the two modalities through direct concatenation, after which algorithms initially intended for unimodal data are applied. However, this rudimentary treatment of multimodal data may lead to substantial bias due to the inherent heterogeneity between different modalities.

To illustrate, consider the concatenated data for the i -th patient represented as $\{w_{i,t}\}_{t \in [T_i]} = (w_{i,1}^{(1)}, \dots, w_{i,T_i^{(1)}}^{(1)}, w_{i,1}^{(2)}, \dots, w_{i,T_i^{(2)}}^{(2)})$, where $T_i = T_i^{(1)} + T_i^{(2)}$. A popular method to handle such data is the SVD-PMI algorithm, as referenced in Levy and Goldberg (2014); Gan

et al. (2025). In this context, we establish the co-occurrence matrices for the concatenated dataset as follows:

$$\mathbf{C} = \begin{bmatrix} \mathbf{C}^{(1,1)} & \mathbf{D}^{(1,2)} \\ \mathbf{D}^{(2,1)} & \mathbf{C}^{(2,2)} \end{bmatrix}.$$

Subsequently, the empirical concatenated PMI matrix, denoted as $\widehat{\mathbb{P}\mathbb{M}\mathbb{I}} = \{\widehat{\mathbb{P}\mathbb{M}\mathbb{I}}(w, w')\}_{w, w' \in [d]}$, is formulated as $\widehat{\mathbb{P}\mathbb{M}\mathbb{I}}(w, w') = \log \frac{\mathbf{C}(w, w')\mathbf{C}(\cdot, \cdot)}{\mathbf{C}(w, \cdot)\mathbf{C}(w', \cdot)}$, where $\mathbf{C}(w, \cdot) = \sum_{w'=1}^d \mathbf{C}(w, w')$ and $\mathbf{C}(\cdot, \cdot) = \sum_{w=1}^d \mathbf{C}(w, \cdot)$. Following this, we conduct a rank- p eigen-decomposition of $\widehat{\mathbb{P}\mathbb{M}\mathbb{I}}$, represented as $\widehat{\mathbf{U}}_{\text{Con}}\widehat{\mathbf{\Lambda}}_{\text{Con}}\widehat{\mathbf{U}}_{\text{Con}}^\top$. The estimator of \mathbf{V}^* is then achieved by setting $\widehat{\mathbf{V}}_{\text{Con}} = \widehat{\mathbf{U}}_{\text{Con}}\widehat{\mathbf{\Lambda}}_{\text{Con}}^{1/2}$. We refer to this method as ‘‘Concat’’.

The second prevalent technique is contrastive learning (CL), applied directly to the concatenated dataset. Specifically, we define the contrastive loss for $\mathbf{V} \in \mathbb{R}^{d \times p}$ as follows:

$$\begin{aligned} \mathcal{L}_{\text{CL}}(\mathbf{V}) = & -\frac{1}{\sum_{i=1}^n T_i(T_i - 1)} \sum_{i=1}^n \sum_{t \in [T_i]} \sum_{s \in [T_i] \setminus \{t\}} \frac{\langle \mathbf{v}_{w_{i,t}}, \mathbf{v}_{w_{i,s}} \rangle}{\gamma_{w_{i,t}} \gamma_{w_{i,s}}} \\ & + \frac{1}{\sum_{i=1}^n \sum_{j:j \neq i}^n T_i T_j} \sum_{i,j:i \neq j} \sum_{t \in [T_i]} \sum_{s \in [T_j]} \frac{\langle \mathbf{v}_{w_{i,t}}, \mathbf{v}_{w_{j,s}} \rangle}{\gamma_{w_{i,t}} \gamma_{w_{j,s}}} + \frac{\lambda}{2} \|\mathbf{V}\mathbf{V}^\top\|_{\text{F}}^2, \end{aligned} \quad (2.5)$$

where $\gamma_w = \mathbf{C}(w, \cdot)$. Let $\widehat{\mathbf{V}}_{\text{CL}} = \arg \min \mathcal{L}_{\text{CL}}(\mathbf{V})$. Similar to Proposition 2.1, we have the following proposition. Here, we define

$$\mathbf{D} = \begin{bmatrix} \mathbf{C}^{(1)} & \mathbf{C}^{(c)} \\ \mathbf{C}^{(c)\top} & \mathbf{C}^{(2)} \end{bmatrix} \text{ with } \mathbf{C}^{(M)}(w, w') = \sum_{i=1}^n \sum_{j:j \neq i}^n \mathbf{C}_{i,j}^{(M,M)}(w, w') \text{ for } w, w' \in \mathcal{W}^{(M)}.$$

Proposition 2.2. *We have $\mathcal{L}_{\text{CL}}(\mathbf{V}) = \frac{\lambda}{2} \left\| \mathbf{V}\mathbf{V}^\top - \frac{1}{\lambda} \widehat{\mathbb{P}\mathbb{M}\mathbb{I}}_{\text{CL}} \right\|_{\text{F}}^2 + (\text{constant})$, where $\widehat{\mathbb{P}\mathbb{M}\mathbb{I}}_{\text{CL}} = \{\widehat{\mathbb{P}\mathbb{M}\mathbb{I}}_{\text{CL}}(w, w')\}_{w, w' \in [d]}$ with*

$$\widehat{\mathbb{P}\mathbb{M}\mathbb{I}}_{\text{CL}}(w, w') := \frac{\mathbf{C}(\cdot, \cdot)\mathbf{C}(\cdot, \cdot)}{\mathbf{C}(w, \cdot)\mathbf{C}(w', \cdot)} \left(\frac{\mathbf{C}(w, w')}{\mathbf{C}(\cdot, \cdot)} - \frac{\mathbf{D}(w, w')}{n(nS_1^{(1)}S_1^{(2)} - S_2^{(1,2)2})} \right).$$

Proposition 2.2 reveals that obtaining $\widehat{\mathbf{V}}_{\text{CL}}$ by minimizing the loss \mathcal{L}_{CL} is essentially equivalent to applying PCA on the matrix $\widehat{\mathbb{P}\mathbb{M}\mathbb{I}}_{\text{CL}}$. The proof for Proposition 2.2 can be found in Supplementary S4.4. This method is referred to as CL. Nevertheless, as we will demonstrate in Section 3, both $\widehat{\mathbf{V}}_{\text{Con}}$ and $\widehat{\mathbf{V}}_{\text{CL}}$ are not optimal solutions.

3 Theoretical Analysis

In this section, we establish the theoretical properties of the proposed CLAIME algorithm and provide a comparative analysis with the two representative baselines discussed in Section 2.3: the simple concatenation approach (Concate) and conventional contrastive learning (CL). Our goal is to articulate the statistical principles that underlie CLAIME, thereby clarifying both why and how it achieves performance gains relative to these alternatives.

3.1 Theoretical Properties of CLAIME

First, we introduce some basic definitions. For $w \in \mathcal{W}^{(M)}$ and $t \in [T_i^{(M)}]$, define $X_{i,w}^{(M)}(t) = \mathbb{I}\{w_{i,t}^{(M)} = w\}$. According to model (2.1), conditioned on \mathbf{c}_i and $\boldsymbol{\epsilon}_i^{(M)} = (\epsilon_{i,w}^{(M)})_{w \in \mathcal{W}^{(M)}}$, the variable $X_{i,w}^{(M)}(t)$ follows a Bernoulli distribution with mean

$$p_{i,w}^{(M)} = \mathbb{E}[X_{i,w}^{(M)}(t) \mid \mathbf{c}_i, \boldsymbol{\epsilon}_i^{(M)}] = \frac{\exp(\langle \mathbf{v}_w^*, \mathbf{c}_i \rangle + \epsilon_{i,w}^{(M)})}{\sum_{w' \in \mathcal{W}^{(M)}} \exp(\langle \mathbf{v}_{w'}^*, \mathbf{c}_i \rangle + \epsilon_{i,w'}^{(M)})}. \quad (3.1)$$

The probability $p_{i,w}^{(M)}$ depends on the discourse vector \mathbf{c}_i and the noise vector $\boldsymbol{\epsilon}_i^{(M)}$, and is independent of t . Let $p_w^{(M)} := \mathbb{E}[p_{i,w}^{(M)}]$.

Next, define the co-occurrence of $w \in \mathcal{W}^{(M)}$ at time t for patient i and $w' \in \mathcal{W}^{(M')}$ at time s for patient j as $X_{i,j,w,w'}^{(M,M')}(t,s) = \mathbb{I}\{w_{i,t}^{(M)} = w, w_{j,s}^{(M')} = w'\}$ for $t \neq s$, with mean $p_{i,j,w,w'}^{(M,M')}$. When $i = j$, define $p_{w,w'}^{(M,M')} := \mathbb{E}[p_{i,i,w,w'}^{(M,M')}]$. For $i \neq j$, we have $\mathbb{E}[p_{i,j,w,w'}^{(M,M')}] = p_w^{(M)} p_{w'}^{(M')}$. We then define the population PMI matrix PMI as

$$\text{PMI} := \begin{pmatrix} \text{PMI}^{(1,1)} & \text{PMI}^{(1,2)} \\ \text{PMI}^{(2,1)} & \text{PMI}^{(2,2)} \end{pmatrix}, \quad \text{PMI}^{(M,M')}(w, w') = \log \frac{p_{w,w'}^{(M,M')}}{p_w^{(M)} p_{w'}^{(M')}} \quad (3.2)$$

for $w \in \mathcal{W}^{(M)}$, $w' \in \mathcal{W}^{(M')}$, and $M, M' \in \{1, 2\}$.

Before proceeding, we clarify our identifiability assumptions. From (2.1), only the left singular space and singular values of \mathbf{V}_1^* and \mathbf{V}_2^* are identifiable. Hence, without loss of

generality, we assume $\mathbf{V}_M^* = \mathbf{U}_M^* \mathbf{\Lambda}_M^*$ for $M \in \{1, 2\}$, where $\mathbf{U}_M^* \in \mathcal{O}_{d_M, p}$ contains the left singular vectors and $\mathbf{\Lambda}_M^* \in \mathbb{R}^{p \times p}$ is diagonal. Model (2.1) is also invariant under the shift $\mathbf{v}_w^* \leftarrow \mathbf{v}_w^* - (1/d_M) \sum_{w' \in \mathcal{W}^{(M)}} \mathbf{v}_{w'}^*$ for all $w \in \mathcal{W}^{(M)}$, and $\mathbf{\Sigma}_M \leftarrow (\mathbf{I} - (1/d_M) \mathbf{1}_{d_M} \mathbf{1}_{d_M}^\top) \mathbf{\Sigma}_M$. Hence, we may also assume $\mathbf{V}_M^{*\top} \mathbf{1}_{d_M} = \mathbf{0}$ and $\mathbf{\Sigma}_M^\top \mathbf{1}_{d_M} = \mathbf{0}$.

Assumption 3.1. For $M \in \{1, 2\}$, assume that $\|\mathbf{U}_M^*\|_{2, \infty} \lesssim \sqrt{p/d_M}$, $\|\mathbf{\Lambda}_M^*\|/s_p(\mathbf{\Lambda}_M^*) \lesssim 1$, and $\|\mathbf{\Lambda}_M^*\| \ll 1$.

Assumption 3.1 is widely known as the incoherence constant condition in the literature appearing in matrix completion (Candès and Recht, 2009), PCA (Zhang et al., 2022), and the analysis of representation learning algorithm (Ji et al., 2023).

Assumption 3.2. Assume that $d_1 \wedge d_2 \gg p \log^2(n+d)$ and $(d_1 \wedge d_2)^2 \gg p^4(d_1 \vee d_2) \log(n+d)$, $n \gg p^2(d_1^2 \vee d_2^2) \log^2(n+d)$, and $n(S_1^{(1)} \wedge S_1^{(2)}) \gg p^2(d_1^6 \vee d_2^6) \log^2(n+d)$.

Assumption 3.2 imposes a condition on the regime of unique features d_1 and d_2 , and the number of patients n . We will discuss the sufficiency of the condition in Remark 3.1. This assumption is technically necessary in bounding the normalizing constant of the model (Lemma S5.2). We introduce the notation $\mathbf{\Sigma} = \text{diag}(\mathbf{\Sigma}_1, \mathbf{\Sigma}_2)$.

Assumption 3.3. Assume that $\|\text{diag}(\mathbf{\Sigma}_M)\|_{\max} \lesssim p/d_M$ for $M \in \{1, 2\}$ and $1/p \ll s_p(\mathbf{\Sigma}) \leq \|\mathbf{\Sigma}_1\| \vee \|\mathbf{\Sigma}_2\| \lesssim 1$.

Assumption 3.3 implies that the signal-to-noise ratio is bounded above and below. Note that the signal, measured by the smallest positive singular value of $(1/p) \mathbf{V}_M^* \mathbf{V}_{M'}^{*\top}$ for $M, M' \in \{1, 2\}$ is of order $1/p$ from Assumption 3.1.

Theorem 3.1. *Under Assumptions 3.1, 3.2 and 3.3, we have*

$$\begin{aligned} \left\| \mathbb{PMI}^{(M,M)} - \left(\frac{1}{p} \mathbf{V}_M^* \mathbf{V}_M^{*\top} + \boldsymbol{\Sigma}_M \right) \right\|_F &\lesssim \frac{p^2}{d_M} \log(n+d), \quad M \in \{1, 2\} \\ \left\| \mathbb{PMI}^{(1,2)} - \frac{1}{p} \mathbf{V}_1^* \mathbf{V}_2^{*\top} \right\|_F &\lesssim \frac{p^2(d_1 \vee d_2)}{(d_1 \wedge d_2)^2} \log(n+d), \quad \text{and hence} \\ \left\| \mathbb{PMI} - \left(\frac{1}{p} \mathbf{V}^* \mathbf{V}^{*\top} + \boldsymbol{\Sigma} \right) \right\|_F &\lesssim \frac{p^2(d_1 \vee d_2)}{(d_1 \wedge d_2)^2} \log(n+d). \end{aligned}$$

The proof of Theorem 3.1 is presented in Supplementary S4.1. It shows that the PMI matrix for each modality can be closely approximated by the product of embeddings plus the noise covariance matrix $\boldsymbol{\Sigma}_M$. When the noise level $\boldsymbol{\Sigma}_M$ is substantial, the PMI value $\mathbb{PMI}^{(M,M)}(w, w')$ for a single modality may significantly deviate from $\langle \mathbf{v}_w^*, \mathbf{v}_{w'}^* \rangle / p$. On the other hand, the cross-modal PMI matrix $\mathbb{PMI}^{(1,2)}$ can be directly approximated by $\mathbf{V}_1^* \mathbf{V}_2^{*\top} / p$. The next theorem affirms that $\widehat{\mathbb{PMI}}_{\text{CLAIME}}$ is an effective estimator for $\mathbb{PMI}^{(1,2)}$.

Assumption 3.4. For $M = 1, 2$, assume that $S_2^{(M)2} \gg S_1^{(M)}$, $S_1^{(M)} \gtrsim S_2^{(M)} \gtrsim S_4^{(M)}$ and $S_2^{(1,2)} \gtrsim S_4^{(1,2)}$. Also assume the non-negative correlation between $(T_i^{(1)})_{i \in [n]}$ and $(T_i^{(2)})_{i \in [n]}$, i.e., $S_2^{(1,2)2} \geq S_1^{(1)} S_1^{(2)}$.

Assumption 3.4 requires that the empirical variance of $T_i^{(M)}$ dominates the mean of $T_i^{(M)}$, and their moments are comparable to each other. For the same length setting $T_i^{(M)} \equiv T^{(M)}$ for all i , the assumption is satisfied if $T^{(M)} \rightarrow \infty$. Assumption 3.4 is satisfied for exponential distribution and gamma distribution with constant order shape parameter.

Theorem 3.2. *Under Assumptions 3.1-3.3 and 3.4, with probability $1 - \exp(-\Omega(\log^2(n+d)))$,*

$$\left\| \widehat{\mathbb{PMI}}_{\text{CLAIME}} - \mathbb{PMI}^{(1,2)} \right\|_F \lesssim \left\{ \frac{d_1^{3/2} d_2^{3/2}}{\sqrt{n}(S_1^{(1)1/2} \wedge S_1^{(2)1/2})} + \frac{d_1^{1/2} d_2^{1/2}}{\sqrt{n}} + \frac{d_1^{1/2} d_2^{1/2} p^2}{(d_1 \wedge d_2)^2} \right\} \log(n+d).$$

The proof of Theorem 3.2 is given in Supplementary S4.3. Under Assumption 3.2, $\widehat{\mathbb{PMI}}_{\text{CLAIME}}$ is an asymptotically unbiased estimate of $\mathbb{PMI}^{(1,2)}$. Combining Theorems 3.1 and 3.2 yields the convergence rate of CLAIME. We also analyze the rate of learning joint

representations via CLAIME. Specifically, we concatenate the left singular vectors of $\widehat{\mathbf{V}}_1$ and $\widehat{\mathbf{V}}_2$. Since $\mathbf{P}_p(\widehat{\mathbf{V}}_1^\top), \mathbf{P}_p(\widehat{\mathbf{V}}_2^\top)$ are only identifiable up to rotation, the subspace spanned by $\mathbf{P}_p([\mathbf{P}_p^\top(\widehat{\mathbf{V}}_1^\top), \mathbf{P}_p^\top(\widehat{\mathbf{V}}_2^\top)])$ depends on the choice of rotations. To address this, we introduce a matrix \mathbf{H} and define the estimated joint representation by $\widehat{\mathbf{U}}_{\mathbf{H}} := \mathbf{P}_p([\mathbf{H}\mathbf{P}_p^\top(\widehat{\mathbf{V}}_1^\top), \mathbf{P}_p^\top(\widehat{\mathbf{V}}_2^\top)])$. We then evaluate performance via $\min_{\mathbf{H} \in \mathcal{O}_{p,p}} \|\sin \Theta(\widehat{\mathbf{U}}_{\mathbf{H}}, \mathbf{U}^*)\|_{\text{F}}$, where $\mathbf{U}^* \in \mathcal{O}_{d,p}$ is the concatenated embedding vectors defined as $\mathbf{U}^* := (1/\sqrt{2})[\mathbf{U}_1^{*\top}, \mathbf{U}_2^{*\top}]$. The proof of Theorem 3.3 is presented in Supplementary S4.3.

Theorem 3.3. *Under Assumptions 3.1-3.4, with probability $1 - \exp(-\Omega(\log^2(n+d)))$,*

$$\begin{aligned} \|\sin \Theta(\mathbf{P}_p(\widehat{\mathbf{V}}_1^\top), \mathbf{U}_1^*)\|_{\text{F}} \vee \|\sin \Theta(\mathbf{P}_p(\widehat{\mathbf{V}}_2^\top), \mathbf{U}_2^*)\|_{\text{F}} &\lesssim \frac{p^3(d_1 \vee d_2) \log(n+d)}{(d_1 \wedge d_2)^2} \\ &+ \frac{pd_1^{3/2}d_2^{3/2} \log(n+d)}{\sqrt{n}(S_1^{(1)1/2} \wedge S_1^{(2)1/2})} + \frac{pd_1^{1/2}d_2^{1/2} \log(n+d)}{\sqrt{n}} \quad \text{and} \end{aligned} \quad (3.3)$$

$$\min_{\mathbf{H} \in \mathcal{O}_{p,p}} \|\sin \Theta(\widehat{\mathbf{U}}_{\mathbf{H}}, \mathbf{U}^*)\|_{\text{F}} \lesssim \left\{ \frac{p^3(d_1 \vee d_2)}{(d_1 \wedge d_2)^2} + \frac{pd_1^{3/2}d_2^{3/2}}{\sqrt{n}(S_1^{(1)1/2} \wedge S_1^{(2)1/2})} + \frac{pd_1^{1/2}d_2^{1/2}}{\sqrt{n}} \right\} \log(n+d).$$

Remark 3.1. The bound in (3.3) consists of a bias term from the nonlinearity of the data-generating process (first term), and two variance terms (last two terms). The first variance term arises from estimating per-record co-occurrence frequencies. Each patient contributes $(T_i^{(1)}, T_i^{(2)})$ -length multimodal data, so the variance of empirical co-occurrence frequencies is $O(1/(n(S_1^{(1)} \wedge S_1^{(2)})))$. Normalizing to obtain PMI entries scales this variance by d_1d_2 , and converting to Frobenius norm adds an extra factor of $d_1^{1/2}d_2^{1/2}$ via the inequality $\|A\|_{\text{F}} \leq d_1^{1/2}d_2^{1/2}\|A\|_{\text{max}}$. Applying the Davis–Kahan theorem then gives a contribution of order $O(pd_1^{3/2}d_2^{3/2}/(n(S_1^{(1)} \wedge S_1^{(2)})))$. The second variance term reflects the averaging across n patients, yielding a $1/\sqrt{n}$ rate, which again is scaled by $d_1^{1/2}d_2^{1/2}$ when converted to Frobenius norm. As a result, to make the overall bound vanish and ensure consistency, Assumption 3.2 is required.

3.2 Comparison with the baseline methods

We now compare CLAI ME with the two baseline approaches introduced in Section 2.3. As discussed there, both baselines can be interpreted as applying SVD to different empirical PMI matrices: the first is SVD on the concatenated PMI matrix $\widehat{\mathbb{P}\text{MII}}$, while the second is based on the estimator $\widehat{\mathbb{P}\text{MII}}_{\text{CL}}$ derived from the CL loss (2.5). We show in Theorem 3.4 (proof in Supplementary S4.4) that both $\widehat{\mathbb{P}\text{MII}}$ and $\widehat{\mathbb{P}\text{MII}}_{\text{CL}}$ are biased estimators of the population matrix $\mathbb{P}\text{MII}$. Building on this result, Theorem 3.5 establishes the convergence rates of the corresponding estimators $\widehat{\mathbf{V}}_{\text{CL}}$ and $\widehat{\mathbf{V}}_{\text{Con}}$, with detailed proofs provided in Supplementary S4.4.

Theorem 3.4. *Under Assumptions 3.1-3.3 and 3.4, with probability $1 - \exp(-\Omega(\log^2(n + d)))$,*

$$\begin{aligned} \left\| \widehat{\mathbb{P}\text{MII}} - (\mathbb{P}\text{MII} + \mathbf{B}_{\text{Con}}) \right\|_{\text{F}} &\lesssim \frac{(d_1 \vee d_2) d_1^2 \log(n + d)}{\sqrt{n} S_1^{(1)1/2}} + \frac{(d_1 \vee d_2) d_2^2 \log(n + d)}{\sqrt{n} S_1^{(2)1/2}} \\ &\quad + \frac{(d_1 \vee d_2) d_1 d_2 \log(n + d)}{\sqrt{n} (S_1^{(1)1/2} \wedge S_1^{(2)1/2})} + \frac{(d_1 \vee d_2) \log(n + d)}{\sqrt{n}}, \quad \text{and} \\ \left\| \widehat{\mathbb{P}\text{MII}}_{\text{CL}} - (\mathbb{P}\text{MII} + \mathbf{B}_{\text{CL}}) \right\|_{\text{F}} &\lesssim \frac{(d_1 \vee d_2) d_1^2 \log(n + d)}{\sqrt{n} S_1^{(1)1/2}} + \frac{(d_1 \vee d_2) d_2^2 \log(n + d)}{\sqrt{n} S_1^{(2)1/2}} \\ &\quad + \frac{(d_1 \vee d_2) d_1 d_2 \log(n + d)}{\sqrt{n} (S_1^{(1)1/2} \wedge S_1^{(2)1/2})} + \frac{\log(n + d) (d_1 \vee d_2)}{\sqrt{n}} + \frac{p^2 (d_1 \vee d_2) \log(n + d)}{(d_1 \wedge d_2)^2}. \end{aligned}$$

Here, \mathbf{B}_{Con} and \mathbf{B}_{CL} are bias matrices defined in Supplementary S4.2 and S4.4.

Remark 3.2. As shown in Theorems S4.2 (Concate) and S4.5 (CL), the bias matrix \mathbf{B}_{CL} includes a correctable term based on observed $T_i^{(M)}$ and an uncorrectable term involving the population-level PMI. In contrast, \mathbf{B}_{Con} depends only on $T_i^{(M)}$ and is fully correctable. To evaluate the effect of this correction, we conducted additional experiments by removing the bias term associated with $T_i^{(M)}$. The results, presented in Supplementary S7.3.3, show that the debiased estimators offer little to no improvement over the original ones, suggesting that the impact of the removable bias component is limited in practice.

Theorem 3.5. Suppose that $\|\mathbf{B}_{\text{Con}}\| \vee \|\mathbf{B}_{\text{CL}}\| \ll 1/p$. Under Assumptions 3.1-3.4, with probability $1 - \exp(-\Omega(\log^2(n+d)))$,

$$\begin{aligned} & \left\| \sin \Theta \left(\mathbf{P}_p(\widehat{\mathbf{V}}_{\text{Con}}^\top), \mathbf{P}_p \left(\frac{1}{p} \mathbf{V}^* \mathbf{V}^{*\top} + \boldsymbol{\Sigma} + \mathbf{B}_{\text{Con}} \right) \right) \right\|_{\text{F}} \\ & \lesssim \frac{p(d_1 \vee d_2) d_1^2 \log(n+d)}{\sqrt{n} S_1^{(1)1/2}} + \frac{p(d_1 \vee d_2) d_2^2 \log(n+d)}{\sqrt{n} S_1^{(2)1/2}} \\ & \quad + \frac{p(d_1 \vee d_2) d_1 d_2 \log(n+d)}{\sqrt{n} (S_1^{(1)1/2} \wedge S_1^{(2)1/2})} + \frac{p \log(n+d) (d_1 \vee d_2)}{\sqrt{n}} + \frac{p^3 (d_1 \vee d_2) \log(n+d)}{(d_1 \wedge d_2)^2}, \\ & \left\| \sin \Theta \left(\mathbf{P}_p(\widehat{\mathbf{V}}_{\text{CL}}^\top), \mathbf{P}_p \left(\frac{1}{p} \mathbf{V}^* \mathbf{V}^{*\top} + \boldsymbol{\Sigma} + \mathbf{B}_{\text{CL}} \right) \right) \right\|_{\text{F}} \\ & \lesssim \frac{p(d_1 \vee d_2) d_1^2 \log(n+d)}{\sqrt{n} S_1^{(1)1/2}} + \frac{p(d_1 \vee d_2) d_2^2 \log(n+d)}{\sqrt{n} S_1^{(2)1/2}} \\ & \quad + \frac{p(d_1 \vee d_2) d_1 d_2 \log(n+d)}{\sqrt{n} (S_1^{(1)1/2} \wedge S_1^{(2)1/2})} + \frac{p \log(n+d) (d_1 \vee d_2)}{\sqrt{n}} + \frac{p^3 (d_1 \vee d_2) \log(n+d)}{(d_1 \wedge d_2)^2}. \end{aligned}$$

Theorem 3.5 shows that both Concatenate and CL will yield biased estimators for the embeddings \mathbf{V}^* due to the inherent bias terms and covariance matrix of the noise. While the bias terms \mathbf{B}_{Con} and \mathbf{B}_{CL} can be partially removed, the influence of $\boldsymbol{\Sigma}$ remains irreducible due to its unobserved nature. Comparing Theorems 3.3 and 3.5, we find that CLAIME achieves a sharper rate than Concatenate and CL even when \mathbf{B}_{CL} , \mathbf{B}_{Con} and $\boldsymbol{\Sigma}$ go to zero. As a result, CLAIME is a better estimator than Concatenate and CL. For the bias terms \mathbf{B}_{Con} and \mathbf{B}_{CL} , we have the following lemma. The proof of Lemma 3.1 is given in Supplementary S4.7.

Lemma 3.1. Suppose that Assumption 3.4 holds. If $T_i^{(1)} = T_i^{(2)}$, then, $\|\mathbf{B}_{\text{Con}}\| \vee \|\mathbf{B}_{\text{CL}}\| \lesssim (d_1 \vee d_2) S_1^{(1)} / S_2^{(1)2}$. Furthermore, if $T_i^{(1)} = T_i^{(2)} \equiv T$ for all $i \in [n]$ for some $T > 0$, then $\|\mathbf{B}_{\text{Con}}\| \vee \|\mathbf{B}_{\text{CL}}\| \lesssim (d_1 \vee d_2) / T$.

We then characterize the effect of $\boldsymbol{\Sigma}$ and show that when $\boldsymbol{\Sigma}$ satisfies suitable conditions, the two existing methods Concatenate and CL will not provide ideal estimators of \mathbf{V}^* .

Assumption 3.5. Assume that $(s_p(\boldsymbol{\Sigma}) - s_{p+1}(\boldsymbol{\Sigma})) / s_p(\boldsymbol{\Sigma}) \gtrsim 1$.

Assumption 3.5 is known as the eigengap condition for the top- p singular vectors of Σ .

A similar assumption has been used in the analysis of contrastive learning (Ji et al., 2023).

This enables us to identify the top- p singular vectors of $(1/p)\mathbf{V}^*\mathbf{V}^{*\top} + \Sigma$.

Assumption 3.6. Assume $\|\sin \Theta(\mathbf{U}_1^*, \mathbf{P}_p(\Sigma_1))\|_F \wedge \|\sin \Theta(\mathbf{U}_2^*, \mathbf{P}_p(\Sigma_2))\|_F \geq \sqrt{(2/3)p}$.

Assumption 3.6 holds if the column space of $\mathbf{P}_p(\Sigma_1)$ is nearly orthogonal to the column space of \mathbf{U}_1^* and that of \mathbf{U}_2^* nearly orthogonal to that of $\mathbf{P}_p(\Sigma_2)$. Roughly speaking, this assumption requires that we can well separate the features and noises based on their directions in each modality.

Theorem 3.6. Suppose $\|\mathbf{B}_{\text{Con}}\| \vee \|\mathbf{B}_{\text{CL}}\| \ll 1/p$. Under Assumptions 3.1-3.6, with probability $1 - \exp(-\Omega(\log^2(n+d)))$, $\|\sin \Theta(\hat{\mathbf{U}}_{\text{Con}}, \mathbf{U}^*)\|_F \gtrsim \sqrt{p}$ and $\|\sin \Theta(\hat{\mathbf{U}}_{\text{CL}}, \mathbf{U}^*)\|_F \gtrsim \sqrt{p}$.

The formal statement is available in Theorem S4.8. Theorem 3.6 shows that there is a huge deviation from the estimators of Concat and CL to the true parameters as $\|\sin \Theta(\hat{\mathbf{U}}_{\text{Con}}, \mathbf{U}^*)\|_F$ and $\|\sin \Theta(\hat{\mathbf{U}}_{\text{CL}}, \mathbf{U}^*)\|_F$ are both lower bounded by the order of \sqrt{p} . Since for any $\hat{\mathbf{U}}, \mathbf{U}^* \in \mathcal{O}_{d,p}$, $\|\sin \Theta(\hat{\mathbf{U}}, \mathbf{U}^*)\|_F$ can be trivially upper bounded by \sqrt{p} , this result shows that $\hat{\mathbf{U}}_{\text{Con}}$ and $\hat{\mathbf{U}}_{\text{CL}}$ can hardly capture any signal in \mathbf{U}^* .

We present an example construction of the error covariance matrix where we expect to see the performance difference among CLAIME, Concat, and CL.

Corollary 3.1. Choose $\mathbf{P}^{(1)} \in \mathcal{O}_{d_1,p}$ satisfying $[\mathbf{U}_1^*; \mathbf{P}^{(1)}] \in \mathcal{O}_{d_1,2p}$ and $\|[\mathbf{U}_1^*; \mathbf{P}^{(1)}]\|_{2,\infty}^2 \lesssim p/d_1$. Similarly choose $\mathbf{P}^{(2)} \in \mathcal{O}_{d_2,p}$ such that $[\mathbf{U}_2^*; \mathbf{P}^{(2)}] \in \mathcal{O}_{d_2,2p}$ and $\|[\mathbf{U}_2^*; \mathbf{P}^{(2)}]\|_{2,\infty}^2 \lesssim p/d_2$. Let $\Sigma_1 := \mathbf{P}^{(1)}\mathbf{P}^{(1)\top}$, $\Sigma_2 := (1/2)\mathbf{P}^{(2)}\mathbf{P}^{(2)\top}$, $\mathbf{V}_1^* = \mathbf{U}_1^*$ and $\mathbf{V}_2^* = \mathbf{U}_2^*$. For these noise covariance matrices, Assumptions 3.1, 3.3 and 3.5 hold. In addition, Assumption 3.6 holds since $\mathbf{P}^{(1)\top}\mathbf{V}_1^* = \mathbf{P}^{(2)\top}\mathbf{V}_2^* = \mathbf{O}_{p \times p}$. Under additional assumptions on $(T_i^{(M)})_{i \in [n]}$, d_1 and d_2

(Assumptions 3.2 and 3.4), with probability $1 - \exp(-\Omega(\log^2(n + d)))$,

$$\begin{aligned} \|\sin \Theta(\hat{\mathbf{U}}_{\text{Con}}, \mathbf{U}^*)\|_{\text{F}} &\gtrsim \sqrt{p}, \quad \|\sin \Theta(\hat{\mathbf{U}}_{\text{CL}}, \mathbf{U}^*)\|_{\text{F}} \gtrsim \sqrt{p} \quad \text{and} \\ \min_{\mathbf{H} \in \mathcal{O}_{p,p}} \|\sin \Theta(\hat{\mathbf{U}}_{\mathbf{H}}, \mathbf{U}^*)\|_{\text{F}} &\lesssim \left\{ \frac{p^3(d_1 \vee d_2)}{(d_1 \wedge d_2)^2} + \frac{pd_1^{3/2}d_2^{3/2}}{\sqrt{n}(S_1^{(1)1/2} \wedge S_1^{(2)1/2})} + \frac{pd_1^{1/2}d_2^{1/2}}{\sqrt{n}} \right\} \log(n + d). \end{aligned}$$

Corollary 3.1 directly follows from Theorems 3.3 and 3.6. Note that the factor $1/2$ in the definition of Σ_2 guarantees the eigengap condition at the p -th largest singular value of the joint noise covariance matrix Σ . The noise covariance in Corollary 3.1 implies that the subspace spanned by the noise is orthogonal to that of the signal, so that noisy fluctuations in the feature frequency distribution occur simultaneously across many features, in a way separable from the signal. Under this condition, Concate and CL tend to learn the eigenspace corresponding to noise covariance matrix, as they are vulnerable to strong noise. In contrast, CLAIME effectively escapes from the noise and recovers the core representations when n and $(d_1 \vee d_2)/(d_1 \wedge d_2)^2$ are sufficiently large.

4 Simulation Studies

In this section, we evaluate the performance of CLAIME and compare it to CL, Concate, and Kernel PCA (KPCA) through simulation studies. KPCA is a nonlinear PCA method that operates in a high-dimensional feature space induced by a kernel function. Following Gupta et al. (2019), we apply KPCA with Gaussian RBF kernel directly to the co-occurrence matrix \mathbf{D} given that the co-occurrence matrix can be viewed as a generalized n -gram similarity matrix. When patient-level data is unavailable, the first three methods can still be applied by performing SVD on various aggregated PMI matrices, as described in Section 2. Since patient-level data is also available in the synthesized datasets, we can additionally apply the gradient descent-based variants: CLAIME-GD and CL-GD, which

optimize the objective functions defined in (2.3) and (2.5), respectively. The suffix “-GD” is added to distinguish them from their SVD-based counterparts. To enhance training efficiency, only 10 negative samples per patient are stochastically sampled. The penalty parameter λ is set to 1, while the learning rate starts at 10^{-4} and decays by a factor of 10 every 10 epochs to ensure convergence. Both gradient-based algorithms converge when their loss functions change by less than 10^{-6} .

We generate a patient embedding vector $\mathbf{c}_i \in \mathbb{R}^p$ for each patient i , independently drawn from a multivariate normal distribution $N(\mathbf{0}, \mathbf{I}_p)$. To construct the code and CUI embedding matrices, we first generate $\mathbf{V}^* = \mathbf{R}\mathbf{M}$, where $\mathbf{M} \in \mathbb{R}^{d \times p}$ has i.i.d. standard normal entries, and $\mathbf{R} \in \mathcal{O}_{d,d}$ is an orthonormal matrix obtained via QR decomposition of a random matrix. The rows of \mathbf{V}^* are mean-centered (i.e., each row has zero mean) and rescaled so that its largest singular value is 1. We then partition \mathbf{V}^* into \mathbf{V}_1^* (first d_1 rows) and \mathbf{V}_2^* (remaining d_2 rows). Performing SVD on \mathbf{V}_1^* and \mathbf{V}_2^* separately yields the column basis matrices \mathbf{U}_1^* and \mathbf{U}_2^* . Next, we generate the data according to model (2.1), where the patient i is assigned $T_i^{(1)}$ codes and $T_i^{(2)}$ CUIs, with $T_i^{(1)}, T_i^{(2)} \sim \text{Poisson}(50)$ truncated to exclude zeros. We consider two different cases for the error covariance structure.

For Case 1, we set $\boldsymbol{\Sigma}^{(M)} = \text{diag}(\mathbf{I}_{p/2}, \mathbf{0})/c \in \mathbb{R}^{d_M \times d_M}$ for $M \in \{1, 2\}$, where $c > 0$ controls the signal-to-noise ratio (SNR) of the data generating process. For Case 2, we generated $\sigma_w \stackrel{i.i.d.}{\sim} \text{Unif}(0, 1)$ and set $\boldsymbol{\Sigma}_{w,w'}^{(M)} = \rho^{|w-w'|} \sigma_w \sigma_{w'}/2$ for $w, w' \in [d_M]$ and $M \in \{1, 2\}$, where $\rho \in (0, 1)$ controls both the structure and the SNR. Specifically, larger ρ values yield higher SNR in the synthesized data.

For both cases, we set $d_1 = d_2 = d/2$ and conduct three experiments to compare the performance of CLAIME, CLAIME-GD, CL, CL-GD, Concat and KPCA under varying sample sizes n , feature sizes d , and SNR. Performance is evaluated using the metric

$\text{Err}(\hat{\mathbf{U}}, \mathbf{U}^*) = \max_{M=1,2} \|\hat{\mathbf{U}}_M \hat{\mathbf{U}}_M^\top - \mathbf{U}_M^* \mathbf{U}_M^{*\top}\|_F$, which measures the subspace distance between estimated and true embeddings. We first fix the SNR by setting $c = 0.2$ for Case 1 and $\rho = 0.8$ for Case 2. In the first experiment, we vary the sample size n in $\{2, 4, 6\} \times 10^4$, while fixing $d = 200$ and $p = 4$. In the second experiment, we vary $d \in \{100, 200, 300, 400\}$, while fixing $n = 2 \times 10^4$ and $p = 4$. For the third experiment, we first fix $n = 2 \times 10^4$, $d = 200$ and $p = 4$. Then, we vary c equally spaced between 0.2 and 0.8 for Case 1, and we vary ρ equally spaced between 0.2 and 0.8 for Case 2.

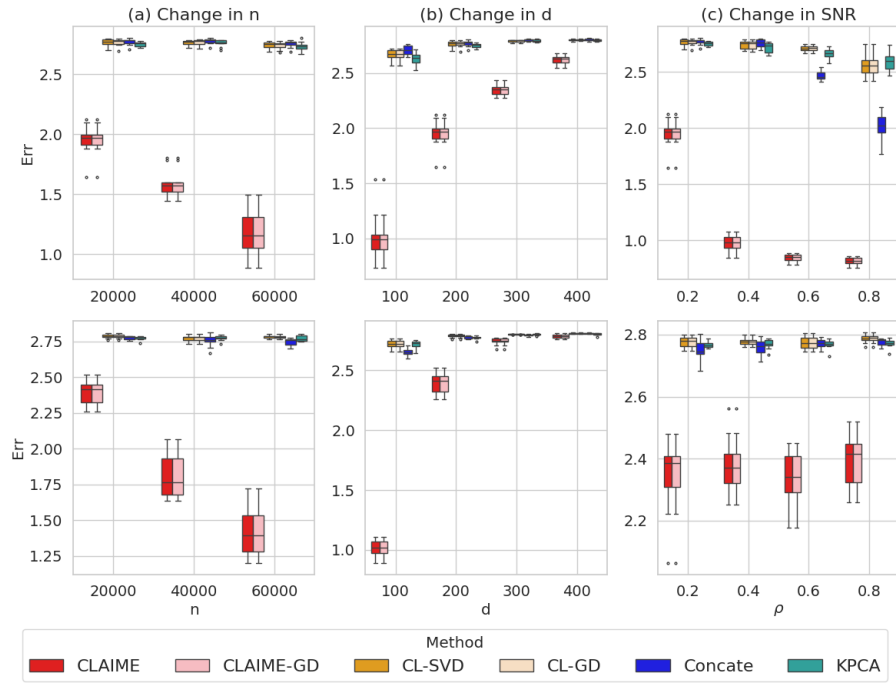


Figure 2: In the top panel, the error metric is plotted against varying n , d and c for Case 1. In the bottom panel, the error metric is plotted against varying n , d and ρ for Case 2.

Boxplots of the error metrics $\text{Err}(\hat{\mathbf{U}}, \mathbf{U}^*)$, averaged over 100 repetitions, are presented in Figure 2. The results for CL and CL-GD, CLAIME and CLAIME-GD are very close to each other, as indicated by the proximity of their lines in Figures 2 (a)–(c). This suggests that employing gradient-based methods on patient-level data (i.e., CL-GD and CLAIME-GD) is comparable to utilizing SVD on summary-level PMI matrices (i.e., CL and CLAIME). This

observation aligns with the theoretical findings in Propositions 2.1 and 2.2. On one hand, in Figures 2(a) and (b), the errors for CLAIME and CLAIME-GD decrease with an increase in n or a decrease in d . This behavior is anticipated and can be theoretically inferred from the upper bounds provided in Theorems 3.1 – 3.3. In contrast, the errors for Concat, CL, and CL-GD remain unchanged. This can be theoretically justified by their lower bounds being irrelevant to both n and d , as shown in Theorem 3.6. Moreover, it can be observed that KPCA behaves similarly to CL and Concat. From the top panel of Figure 2(c), we observe that all methods incur larger errors as c decreases—that is, as the SNR worsens. Compared to the other methods, CLAIME and CLAIME-GD consistently demonstrate superior performance. This finding supports our initial motivation: the proposed method is more robust in noisier data settings. Similarly, in the bottom panel of Figure 2(c), while other methods exhibit only a slight decline in performance as ρ decreases, CLAIME and CLAIME-GD again significantly outperform the alternatives across all values of ρ .

We conducted additional simulation experiments in Supplementary S7.3.1 and S7.3.2 to empirically examine larger d and account for model misspecification. Similar patterns were observed, demonstrating the robustness of our methods across broader settings. Furthermore, in Supplementary S7.3.3, we compared our approach against the Concat and CL methods with debiasing (Remark 3.2), and our method continued to outperform them.

5 Application to Electronic Health Records Studies

We train a joint representation of codified and narrative CUI features using summary EHR data of patients with at least 1 diagnostic code of Rheumatoid Arthritis (RA) at Mass General Brigham (MGB). The MGB RA EHR cohort consists of 53,716 patients whose longitudinal EHR data have been summarized as co-occurrence counts of EHR concepts

within a 30-day window. We include all EHR diagnosis, medication, and procedure codes which have been rolled up to higher concept levels: diagnostic codes to PheCodes¹, procedure codes to clinical classification system (CCS)², medication codes to ingredient level RxNorm codes (Liu et al., 2005). We include all EHR codified features along with CUIs that have occurred more than 15 times in the cohort. This results in $d = 4,668$ features, including $d_1 = 3,477$ codified features with 1,776 PheCodes for diseases, 238 CCS codes for procedures, and 1,463 RxNorm codes for medications, and $d_2 = 1,048$ CUI features.

Based on the summary-level co-occurrence matrix, we can derive estimators for CLAIME, CL, Concate and KPCA, respectively. To assess the quality of the obtained embeddings, we utilize a benchmark previously introduced in Gan et al. (2025). For multimodal learning, we are interested in our method’s ability to capture cross modality relationships. Specifically, we first assess the similarity between mapped code-CUI pairs, leveraging UMLS to map codified concepts to CUIs. For relatedness, we first curate UMLS relationships for CUI-CUI pairs, considering major classes like “may treat or may prevent”, “classifies”, “differential diagnosis”, “method of”, and “causative”. Then, we map disease CUIs to PheCodes, drugs to RxNorm, and procedures to CCS categories to obtain related code-CUI pairs. These mapped code pairs are then utilized to evaluate the system’s ability to detect relatedness between codified and NLP features.

To assess different relationship types, we compute cosine similarities between embedding vectors of known and randomly selected pairs. This enables calculation of the Area Under the Curve (AUC), quantifying how well the embeddings distinguish known pairs from random ones. Random pairs are matched on semantic type; for instance, when evaluating the “may treat or may prevent” relationship, we consider only disease–drug pairs. This

¹<https://phewascatalog.org/phecodes>

²https://www.hcup-us.ahrq.gov/toolssoftware/ccs_svcsproc/ccssvcproc.jsp

strategy allows us to compare embedding performance across relationship types.

Type	Group	CLAIME	CL	Concate	KPCA	Number of known pairs
Similar	CUI-PheCode	0.910	0.911	0.911	0.916	345
	CUI-RxNorm	0.944	0.898	0.900	0.986	49
Related	May Treat (Prevent)	0.775	0.753	0.753	0.711	1302
	Classifies	0.905	0.895	0.895	0.887	744
	ddx	0.773	0.766	0.765	0.670	1169
	Causative	0.775	0.742	0.741	0.695	524

Table 1: AUCs of between-vector cosine similarity in detecting known similar or related pairs of codes vs CUIs for embeddings trained by different methods.

The results in Table 1 show that all methods are more effective at identifying similar pairs than related ones, as indicated by consistently higher AUCs in the “Similar” category. Among the methods, KPCA performs best for detecting similarity, achieving the highest AUCs for both CUI-PheCode and CUI-RxNorm pairs. However, when it comes to the more challenging task of detecting relatedness, the proposed CLAIME method consistently outperforms the baselines, especially KPCA. Notably, CLAIME shows a substantial advantage in identifying causative relationships, with an approximate 3.3% AUC improvement over CL and Concat, and an 8% gain over KPCA. These results underscore CLAIME’s robustness in capturing complex and nuanced associations between medical concepts.

Since the data comes from the RA cohort, it is of interest for us to further perform case studies for RA-related codified and CUI concepts. We select 7 key concepts for detailed analysis: rheumatoid arthritis (RA), C-reactive proteins (CP), stiffness of joint (SoJ), Reiter’s disease (RD), swollen joint (SJ), pneumococcal vaccine (PV), and leflunomide (LF). For each of the 7 concepts, we calculate its cosine similarity with all remaining concepts using the embeddings generated by CLAIME, Concate, and CL, respectively.

Concepts are ranked by similarity, and a subset comprising the top-100 rankings from any one of the three methods is chosen as positive control. Then, we randomly select an equal number of other concepts as negative controls. This process produces an evaluation set for each of the 7 concepts. Concordance between similarity scores (from CLAIME, Concate, CL) and relevance scores (from GPT3.5 (OpenAI, 2023), GPT4 (Achiam et al., 2023)) is assessed using Kendall’s tau rank correlation. Relevance scores are obtained by prompting GPT3.5 and GPT4 to rate concept relevance on a scale of 0 to 1 between the given concept and its respective evaluation set. The detailed prompt is given in Supplementary S7.1.

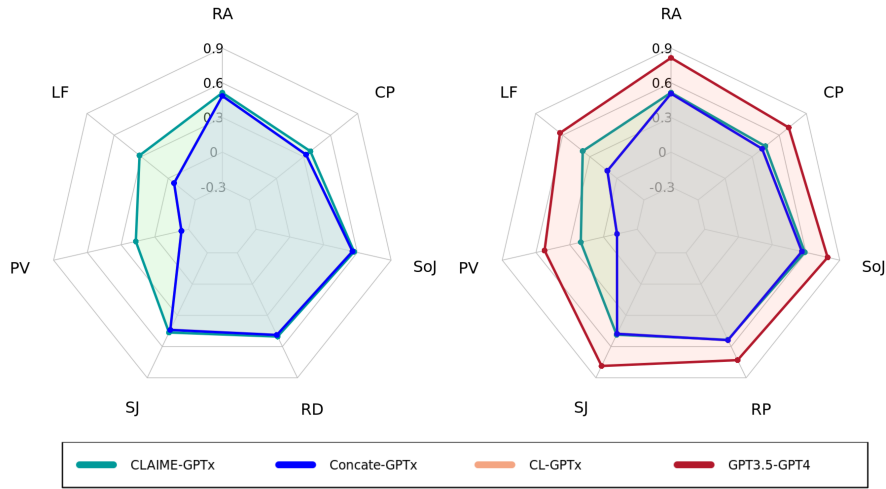


Figure 3: Feature-specific Kendall’s rank correlations between CLAIME, Concate, and CL with GPT-3.5 and GPT-4 scores for 7 concepts. ‘GPTx’ denotes GPT-3.5 (left) and GPT-4 (right); note that CL-GPTx overlaps with Concate-GPTx and is not visible in the figure.

The results, depicted in Figure 3, reveal that Concate and CL exhibit remarkably similar behavior, with the “CL-GPTx” lines obscured beneath “Concate-GPTx”. CLAIME can effectively encode and preserve relations between these medical concepts and their associated features. Notably, negative rank correlations can be observed for CL-GPT3.5/4 and Concate-GPT3.5/4 regarding “leflunomide” and “pneumococcal vaccine” related codes

and CUIs. To gain more insights, some detailed examples are provided in Table S1 in Supplementary S7.1.

As shown in Supplementary S6, CLAIME achieved strong performance when partitioning data elements into five modalities: diagnoses, procedures, medications, lab results, and CUIs. Its advantage is most evident in evaluating related relationships, with particularly pronounced improvements for ‘causative,’ ‘classifies,’ and ‘method of’ associations.

6 Discussion and Conclusion

In this paper, we propose the noisy multimodal log-linear production model for analyzing multimodal EHR data and present the privacy-preserving algorithm CLAIME for estimating multimodal feature embeddings with theoretical justification. Our algorithm is readily applicable to federated learning when multiple healthcare systems wish to co-train their models without sharing patient-level data. It is also of great interest to consider settings where different systems have overlapping but non-identical feature sets, in which case block-wise matrix completion techniques may be useful (Zhou et al., 2023).

While our main development focuses on the two-modality setting, CLAIME is conceptually extensible to more than two modalities, as illustrated in Supplementary S6. Theoretical justification, however, remains challenging. A central insight of our work is that, in the two-modality case, the loss function admits a closed-form global minimizer directly connected to the SVD of the PMI matrix. This reduction is crucial: it allows us to analyze the performance of the CLAIME representation through the top- p singular space of $\widehat{\text{PMI}}_{\text{CLAIME}}$. By contrast, the straightforward multimodal extension lacks such an explicit form, making the global minimizer analytically intractable.

This limitation reflects a broader challenge in the theory of contrastive learning, where

rigorous analyses remain largely confined to the two-view case (Nakada et al., 2023; Dumier et al., 2024). Moreover, our current extension assumes access only to pairwise co-occurrence matrices (Finlayson et al., 2014; Beam et al., 2020). If patient-level data were available, one could, in principle, construct higher-order co-occurrence tensors that capture joint dependencies across three or more modalities. Tensor SVD or related decompositions could then provide a natural way to generalize CLAIME embeddings with accompanying theoretical guarantees. Such a tensor-based framework could reveal interactions that are invisible to pairwise models, for example uncovering clinical pathways that involve coordinated use of lab tests, diagnoses, and treatments. Developing the statistical theory and scalable algorithms for such tensor-based generalizations remains an important direction for future work.

Beyond the linear loss considered here, exploring nonlinear losses such as those in Remark 2.2 is a natural next step. While a linear inner-product model captures only additive associations between modalities, nonlinear mappings (e.g., replacing the bilinear form $\mathbf{V}_1 \mathbf{V}_2^\top$ with a neural network) could model richer dependencies. However, ensuring identifiability and statistical guarantees would require new theory beyond classical low-rank approximation, making the balance between flexibility, interpretability, and tractability a key open challenge. Another promising direction is the estimation of patient embeddings \mathbf{c}_i , which could enable clustering into clinically meaningful subgroups, modeling disease trajectories, and powering personalized applications such as “patients like me” recommendations. Such embeddings may be derived through joint factorization of patient–feature co-occurrence matrices or by incorporating temporal information from longitudinal data, with a theoretical framework for their statistical properties—consistency, stability, and generalization—being essential to ensure reliability in practice.

References

- Achiam, J., Adler, S., Agarwal, S., Ahmad, L., Akkaya, I., Aleman, F. L., Almeida, D., Altenschmidt, J., Altman, S., Anadkat, S., et al. (2023). GPT-4 technical report. *arXiv preprint arXiv:2303.08774*.
- Alsentzer, E., Murphy, J. R., Boag, W., Weng, W.-H., Jin, D., Naumann, T., and McDermott, M. (2019). Publicly available clinical bert embeddings. *arXiv preprint arXiv:1904.03323*.
- Arora, S., Li, Y., Liang, Y., Ma, T., and Risteski, A. (2016). A latent variable model approach to pmi-based word embeddings. *Transactions of the Association for Computational Linguistics*, 4:385–399.
- Arora, S., Li, Y., Liang, Y., Ma, T., and Risteski, A. (2018). Linear algebraic structure of word senses, with applications to polysemy. *Transactions of the Association for Computational Linguistics*, 6:483–495.
- Arora, S., Liang, Y., and Ma, T. (2017). A simple but tough-to-beat baseline for sentence embeddings. In *International Conference on Learning Representations*.
- Bardak, B. and Tan, M. (2021). Improving clinical outcome predictions using convolution over medical entities with multimodal learning. *Artificial Intelligence in Medicine*, 117:102112.
- Beam, A. L., Kompa, B., Schmaltz, A., Fried, I., Weber, G., Palmer, N., Shi, X., Cai, T., and Kohane, I. S. (2019). Clinical concept embeddings learned from massive sources of multimodal medical data. In *PACIFIC SYMPOSIUM ON BIOCOMPUTING 2020*, pages 295–306. World Scientific.
- Beam, A. L., Kompa, B., Schmaltz, A., Fried, I., Weber, G., Palmer, N., Shi, X., Cai, T., and Kohane, I. S. (2020). Clinical concept embeddings learned from massive sources of multimodal medical data. In *Pacific Symposium on Biocomputing. Pacific Symposium on Biocomputing*, volume 25, page 295.
- Candès, E. J. and Recht, B. (2009). Exact matrix completion via convex optimization. *Foundations of Computational Mathematics*, 9(6):717–772.
- Choi, E., Bahadori, M. T., Searles, E., Coffey, C., Thompson, M., Bost, J., Tejedor-Sojo, J., and Sun, J. (2016a). Multi-layer representation learning for medical concepts. In *Proceedings of the 22nd ACM SIGKDD International Conference on Knowledge Discovery and Data Mining*, pages 1495–1504.

- Choi, E., Schuetz, A., Stewart, W. F., and Sun, J. (2017). Using recurrent neural network models for early detection of heart failure onset. *Journal of the American Medical Informatics Association*, 24(2):361–370.
- Choi, Y., Chiu, C. Y.-I., and Sontag, D. (2016b). Learning low-dimensional representations of medical concepts. *AMIA Summits on Translational Science Proceedings*, 2016:41–50.
- Collins, M., Dasgupta, S., and Schapire, R. E. (2001). A generalization of principal components analysis to the exponential family. *Advances in Neural Information Processing Systems*, 14.
- De Vine, L., Zuccon, G., Koopman, B., Sitbon, L., and Bruza, P. (2014). Medical semantic similarity with a neural language model. In *Proceedings of the 23rd ACM International Conference on Information and Knowledge Management*, pages 1819–1822.
- Deng, Y., Prasad, K., Fernandez, R., Smolensky, P., Chaudhary, V., and Shieber, S. (2023). Implicit chain of thought reasoning via knowledge distillation. *arXiv preprint arXiv:2311.01460*.
- Devlin, J., Chang, M., Lee, K., and Toutanova, K. (2019). BERT: pre-training of deep bidirectional transformers for language understanding. In *Proceedings of the 2019 Conference of the North American Chapter of the Association for Computational Linguistics: Human Language Technologies, NAACL-HLT*, pages 4171–4186.
- Dufumier, B., Castillo-Navarro, J., Tuia, D., and Thiran, J.-P. (2024). What to align in multimodal contrastive learning? *arXiv preprint arXiv:2409.07402*.
- Feng, Q., Jiang, M., Hannig, J., and Marron, J. (2018). Angle-based joint and individual variation explained. *Journal of Multivariate Analysis*, 166:241–265.
- Finlayson, S. G., LePendou, P., and Shah, N. H. (2014). Building the graph of medicine from millions of clinical narratives. *Scientific data*, 1(1):1–9.
- Gan, Z., Zhou, D., Rush, E., Panickan, V. A., Ho, Y.-L., Ostrouchovm, G., Xu, Z., Shen, S., Xiong, X., Greco, K. F., et al. (2025). Arch: Large-scale knowledge graph via aggregated narrative codified health records analysis. *Journal of Biomedical Informatics*, page 104761.

- Gupta, V., Giesselbach, S., Rüping, S., and Bauckhage, C. (2019). Improving word embeddings using kernel pca. In *Proceedings of the 4th Workshop on Representation Learning for NLP (RepL4NLP-2019)*, pages 200–208.
- Gutmann, M. and Hyvärinen, A. (2010). Noise-contrastive estimation: A new estimation principle for unnormalized statistical models. In *Proceedings of the thirteenth international conference on artificial intelligence and statistics*, pages 297–304. JMLR Workshop and Conference Proceedings.
- Halpern, Y., Horng, S., Choi, Y., and Sontag, D. (2016). Electronic medical record phenotyping using the anchor and learn framework. *Journal of the American Medical Informatics Association*, 23(4):731–740.
- Hinton, G. E. and Salakhutdinov, R. R. (2006). Reducing the dimensionality of data with neural networks. *Science*, 313(5786):504–507.
- Hong, C., Rush, E., Liu, M., Zhou, D., Sun, J., Sonabend, A., Castro, V. M., Schubert, P., Panickan, V. A., Cai, T., et al. (2021). Clinical knowledge extraction via sparse embedding regression (KESER) with multi-center large scale electronic health record data. *NPJ digital medicine*, 4(1):1–11.
- Huang, K., Singh, A., Chen, S., Moseley, E., Deng, C.-Y., George, N., and Lindvall, C. (2020). Clinical XLNet: Modeling sequential clinical notes and predicting prolonged mechanical ventilation. In *Proceedings of the 3rd Clinical Natural Language Processing Workshop*, pages 94–100, Online. Association for Computational Linguistics.
- Huang, Y., Du, C., Xue, Z., Chen, X., Zhao, H., and Huang, L. (2021). What makes multi-modal learning better than single (provably). *Advances in Neural Information Processing Systems*, 34:10944–10956.
- Ji, W., Deng, Z., Nakada, R., Zou, J., and Zhang, L. (2023). The power of contrast for feature learning: A theoretical analysis. *Journal of Machine Learning Research*, 24(330):1–78.
- Johnson, A. E., Pollard, T. J., Shen, L., Lehman, L.-w. H., Feng, M., Ghassemi, M., Moody, B., Szolovits, P., Anthony Celi, L., and Mark, R. G. (2016). MIMIC-III, a freely accessible critical care database. *Scientific Data*, 3(1):1–9.
- Kartchner, D., Christensen, T., Humpherys, J., and Wade, S. (2017). Code2vec: Embedding and clustering

- medical diagnosis data. In *2017 IEEE International Conference on Healthcare Informatics (ICHI)*, pages 386–390.
- Khadanga, S., Aggarwal, K., Joty, S., and Srivastava, J. (2019). Using clinical notes with time series data for ICU management. In Inui, K., Jiang, J., Ng, V., and Wan, X., editors, *Proceedings of the 2019 Conference on Empirical Methods in Natural Language Processing and the 9th International Joint Conference on Natural Language Processing (EMNLP-IJCNLP)*, pages 6432–6437, Hong Kong, China. Association for Computational Linguistics.
- Lehman, E. and Johnson, A. (2023). Clinical-t5: Large language models built using mimic clinical text. *PhysioNet*.
- Levy, O. and Goldberg, Y. (2014). Neural word embedding as implicit matrix factorization. In *Advances in Neural Information Processing Systems*, volume 27.
- Li, R. and Gao, J. (2022). Multi-modal contrastive learning for healthcare data analytics. In *2022 IEEE 10th International Conference on Healthcare Informatics (ICHI)*, pages 120–127. IEEE.
- Liu, S., Ma, W., Moore, R., Ganesan, V., and Nelson, S. (2005). RxNorm: prescription for electronic drug information exchange. *IT Professional*, 7(5):17–23.
- Liu, S., Wang, X., Hou, Y., Li, G., Wang, H., Xu, H., Xiang, Y., and Tang, B. (2022). Multimodal data matters: language model pre-training over structured and unstructured electronic health records. *IEEE Journal of Biomedical and Health Informatics*, 27(1):504–514.
- Lock, E. F., Hoadley, K. A., Marron, J. S., and Nobel, A. B. (2013). Joint and individual variation explained (jive) for integrated analysis of multiple data types. *The annals of applied statistics*, 7(1):523.
- Lu, J., Yin, J., and Cai, T. (2023). Knowledge graph embedding with electronic health records data via latent graphical block model. *arXiv preprint arXiv:2305.19997*.
- McInnes, B. T., Pedersen, T., and Carlis, J. (2007). Using UMLS Concept Unique Identifiers (CUIs) for word sense disambiguation in the biomedical domain. In *AMIA Annual Symposium Proceedings*, volume 2007, pages 533–537. American Medical Informatics Association.

- Mikolov, T., Chen, K., Corrado, G., and Dean, J. (2013). Efficient estimation of word representations in vector space. *Proceedings of Workshop at ICLR*, 2013.
- Nakada, R., Gulluk, H. I., Deng, Z., Ji, W., Zou, J., and Zhang, L. (2023). Understanding multimodal contrastive learning and incorporating unpaired data. In *International Conference on Artificial Intelligence and Statistics*, pages 4348–4380. PMLR.
- Oord, A. v. d., Li, Y., and Vinyals, O. (2018). Representation learning with contrastive predictive coding. *arXiv preprint arXiv:1807.03748*.
- OpenAI (2023). ChatGPT: Optimizing language models for dialogue. URL: <https://openai.com/blog/chatgpt>.
- Qiao, Z., Wu, X., Ge, S., and Fan, W. (2019). Mnn: multimodal attentional neural networks for diagnosis prediction. *Extraction*, 1(2019):A1.
- Radford, A., Kim, J. W., Hallacy, C., Ramesh, A., Goh, G., Agarwal, S., Sastry, G., Askell, A., Mishkin, P., Clark, J., et al. (2021). Learning transferable visual models from natural language supervision. In *International Conference on Machine Learning*, pages 8748–8763. PMLR.
- Scheurwegs, E., Luyckx, K., Luyten, L., Daelemans, W., and Van den Bulcke, T. (2016). Data integration of structured and unstructured sources for assigning clinical codes to patient stays. *Journal of the American Medical Informatics Association*, 23(e1):e11–e19.
- Sheikhalishahi, S., Miotto, R., Dudley, J. T., Lavelli, A., Rinaldi, F., Osmani, V., et al. (2019). Natural language processing of clinical notes on chronic diseases: systematic review. *JMIR Medical Informatics*, 7(2):e12239.
- Stang, P. E., Ryan, P. B., Racoosin, J. A., Overhage, J. M., Hartzema, A. G., Reich, C., Welebob, E., Scarnecchia, T., and Woodcock, J. (2010). Advancing the science for active surveillance: rationale and design for the observational medical outcomes partnership. *Annals of Internal Medicine*, 153(9):600–606.
- Wang, X., Luo, J., Wang, J., Yin, Z., Cui, S., Zhong, Y., Wang, Y., and Ma, F. (2023). Hierarchical pretraining on multimodal electronic health records. In *Proceedings of the Conference on Empirical*

- Methods in Natural Language Processing. Conference on Empirical Methods in Natural Language Processing*, volume 2023, page 2839.
- Xu, Z., Gan, Z., Zhou, D., Shen, S., Lu, J., and Cai, T. (2023). Inference of dependency knowledge graph for electronic health records. *arXiv preprint arXiv:2312.15611*.
- Yang, Z. and Michailidis, G. (2016). A non-negative matrix factorization method for detecting modules in heterogeneous omics multi-modal data. *Bioinformatics*, 32(1):1–8.
- Yi, S., Wong, R. K. W., and Gaynanova, I. (2023). Hierarchical nuclear norm penalization for multi-view data integration. *Biometrics*, 79(4):2933–2946.
- Yin, Q., Zhong, L., Song, Y., Bai, L., Wang, Z., Li, C., Xu, Y., and Yang, X. (2023). A decision support system in precision medicine: contrastive multimodal learning for patient stratification. *Annals of Operations Research*, pages 1–29.
- Zhang, A. R., Cai, T. T., and Wu, Y. (2022). Heteroskedastic PCA: Algorithm, optimality, and applications. *The Annals of Statistics*, 50(1):53–80.
- Zhang, Z., Liu, J., and Razavian, N. (2020). BERT-XML: Large scale automated ICD coding using BERT pretraining. In Rumshisky, A., Roberts, K., Bethard, S., and Naumann, T., editors, *Proceedings of the 3rd Clinical Natural Language Processing Workshop*, pages 24–34, Online. Association for Computational Linguistics.
- Zhou, D., Cai, T., and Lu, J. (2023). Multi-source learning via completion of block-wise overlapping noisy matrices. *Journal of Machine Learning Research*, 24(221):1–43.
- Zhou, D., Gan, Z., Shi, X., Patwari, A., Rush, E., Bonzel, C.-L., Panickan, V. A., Hong, C., Ho, Y.-L., Cai, T., et al. (2022). Multiview incomplete knowledge graph integration with application to cross-institutional EHR data harmonization. *Journal of Biomedical Informatics*, 133:104147.
- Zhou, G., Cichocki, A., Zhang, Y., and Mandic, D. P. (2015). Group component analysis for multiblock data: Common and individual feature extraction. *IEEE Transactions on Neural Networks and Learning Systems*, 27(11):2426–2439.